# Rheology of Guar Solutions

PATRICK J. WHITCOMB, JOHN GUTOWSKI, and WARREN W. HOWLAND, *Henkel Corporation, Minneapolis, Minnesota 55413*

## Synopsis

The rheology of aqueous solutions of guar is studied over a wide range of shear rates and concentrations. At sufficiently low and high shear rates guar solutions show regions of Newtonian behavior, while at intermediate shear rates they are pseudoplastic. Preliminary normal stress data, and the effects of salt concentration are discussed. Molecular size distribution profiles of hydrated guar, obtained by low pressure (20 psig) filtration through Nucleopore filter membranes, are discussed in terms of guar purity.

## INTRODUCTION

This study was undertaken to expand the understanding of guar solutions through the characterization of the flow properties of the galactomannan (polymeric) portion of guar, termed guaran.

Guar gum is a high-molecular-weight naturally occurring polysaccharide.[1] It consists mostly of linear polymannan with single galactose unit side chains,[1] (Fig. 1). The chemical structure and high molecular weight of these molecules give guar its thickening properties. Many commercial applications of guar are based primarily on its ability to modify a system's flow properties (rheology). Knowledge of the rheological behavior of guar is essential in meeting end-user requirements. Guar's rheology is generally determined from viscosity measurements. Since guar solutions are pseudoplastic (shear thinning), viscosity measurements must be done over a wide range of shear rate. We have characterized the rheology of aqueous guar solutions over wide ranges of shear rates and concentrations.

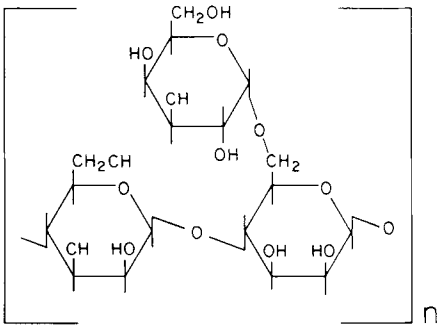


Fig. 1. Proposed average unit structure of guar[1] (MW = 486).

Journal of Applied Polymer Science, Vol. 25, 2815–2827 (1980)

0021-8995/80/0025-2815$01.30

## EXPERIMENTAL

Plant variety and method of extraction affect guar gum composition, e.g., the content of galactomannan, protein, fiber. To minimize these compositional differences, we attempted to obtain a sample as nearly as practical of 100% galactomannan. The starting material was processed guar flour, i.e., crude guar. This was extracted with alcohol in a Soxhlet extractor to remove soluble fat and protein, then dissolved in water, and filtered through an 8-$\mu$m pore diam Nucleopore filter membrane (Nucleopore Corp.) to remove insoluble material, such as cellulose. The purification procedure is explained in more detail in paragraphs latter on in this article. Care was taken not to degrade the polymer portion of guar during purification by maintaining a low extraction temperature, minimizing shear on the polymer, and limiting the oxygen contact with the polymer. The flow properties of the purified guar (98.9% poly galactomannan) were studied.

Hydrodynamic particle size distribution profiles[2] were used to characterize the guar gum at various stages of purification. We assume that owing to rapid Brownian motion, hydrated guar particles can be represented in solution as spheres whose diameters equal the largest dimension of the particle. This dimension will control passage through the pores and is what we term hydrodynamic particle size. This assumption appears to be valid as the ratio of Brownian time to flow time through a pore is approximately $1.3 \times 10^{-14}$.

Samples for hydrodynamic particle size distribution plots were prepared by dispersing the guar in the water using a Waring Blendor. By keeping the Blendor speed as low as possible, the shear and oxygen entrainment were minimized, yet the polymer was thoroughly wetted and no lumps were formed. Mixing time was also kept to a minimum of ~30 sec. The solution was then transferred to a beaker and mixed on a magnetic stirrer, typically for 18 hr. Next 25-ml aliquots of this stock guar solution were removed and placed in a Millipore pressure filtration cell (Millipore Corp.) equipped with 47-mm diam Nucleopore filter membranes of various pore diameters, ranging from 12 to 0.03 $\mu$m. The cell was

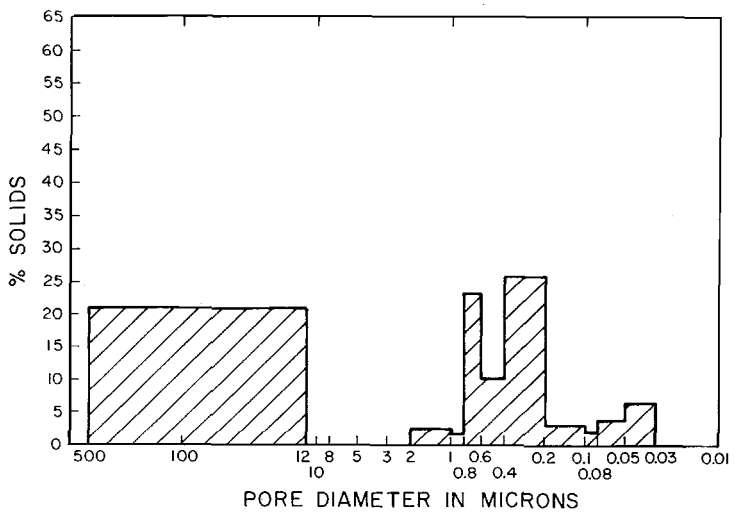


Fig. 2. Unpurified guar in water (percent total solids at each filtration stage vs. pore diam).

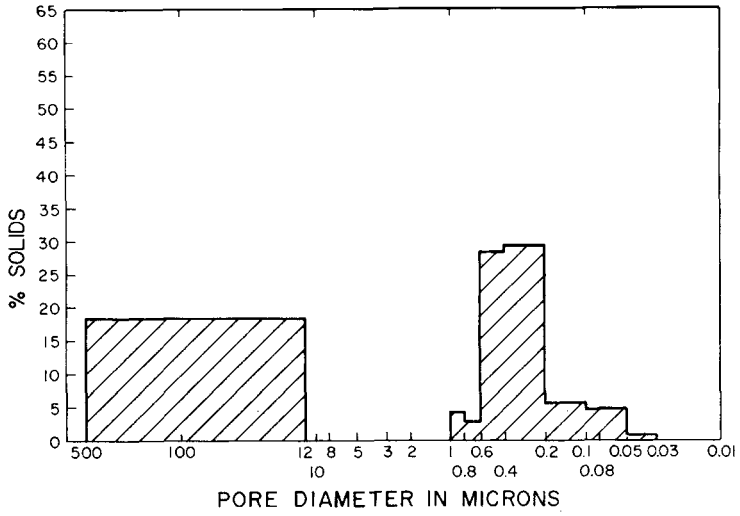


Fig. 3. Guar extracted with EtOH in water (percent total solids at each filtration stage vs. pore diam).

sealed and pressurized to 138 kPa. A minimum of 10 ml of filtrate was collected over a period of time ranging from 5 sec for a 12-$\mu$m pore diam to 18 hr for a pore diameter of 0.03 $\mu$m. Each sample was weighed to the nearest $1/10$ mg. The water was then removed by evaporation in a dust-free oven. The residue was weighed and the solids level of the filtrate calculated. Figure 2 shows a distribution plot of the hydrodynamic particle size of unpurified guar as determined by Nucleopore pore diameters of 12, 10, 8, 5, 3, 2, 1, 0.8, 0.6, 0.4, 0.2, 0.1, 0.08, 0.05, and 0.03 $\mu$m.

The purification of the guar was accomplished in two steps. The first step

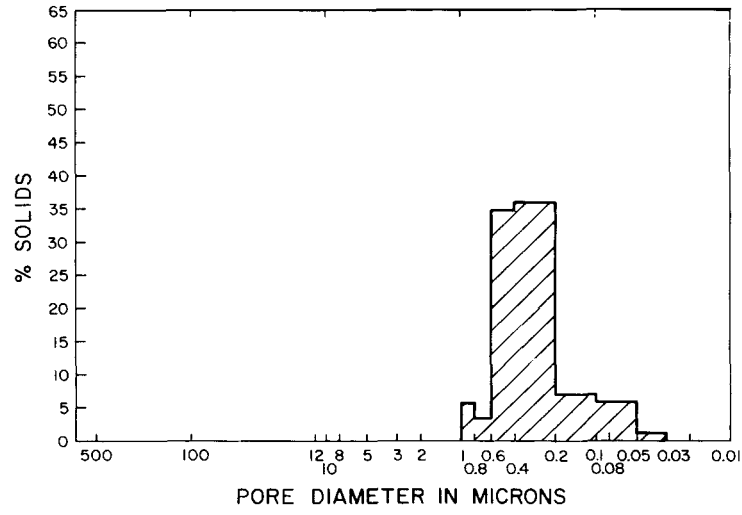


Fig. 4. Purified guar (extracted with EtOH and filtered through 8-$\mu$m pore diam Nucleopore membrane) in water (percent total solids at each filtration stage vs. pore diam).

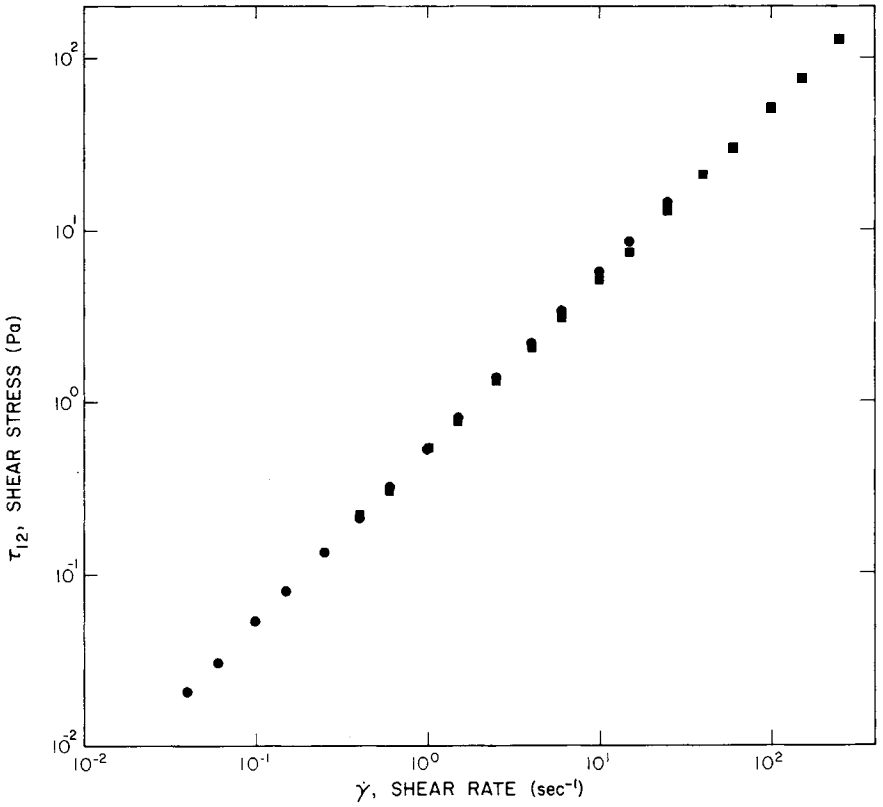


Fig. 5. Silicone oil: ●, sensitive transducer; ■, normal transducer.

was a five-day Soxhlet extraction using 95% ethanol at an average temperature of only 64°C to remove soluble protein and fat. Comparing the partially purified guar (Fig. 3) to the unpurified guar (Fig. 2), two major differences can be seen.

TABLE I
Typical Shear Rates

| $\dot{\gamma}$, $sec^{-1}$ | Phenomena |
|---|---|
| <0.1 | Film sag or film flow on a vertical plate |
| 0.1–10 | Compression molding |
| | Normal range for Brookfield readings |
| 10–100 | Tumbling or pouring |
| | Calendering |
| | Shear rate encountered in the mouth during chewing |
| 100–1000 | Home mixers |
| | Extrusion |
| 1000–10 000 | Waring Blendor |
| | Injection molding |
| >10 000 | Colloid mill |
| | Drilling |

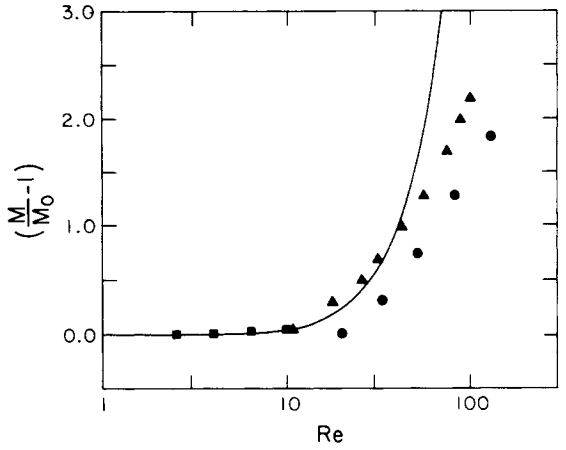


Fig. 6. Turian's correction[7]: (—) $M/M_0 - 1 = 3/4900\ Re^2$; ▲, Cheng; ■, 10-cS oil; (●) water; 0.04-rad cone.

There is a shift from the 0.8- to 0.6-$\mu$m portion to the 0.6- to 0.4-$\mu$m portion, possibly because of unraveling of bundles of guar molecules by hydrogen bond disruption. Also, there is a large reduction of the 0.05- to 0.03-$\mu$m portion, probably because of the denaturization and/or removal of protein. The total weight loss of the sample was only 4.7%, whereas the protein level (as determined

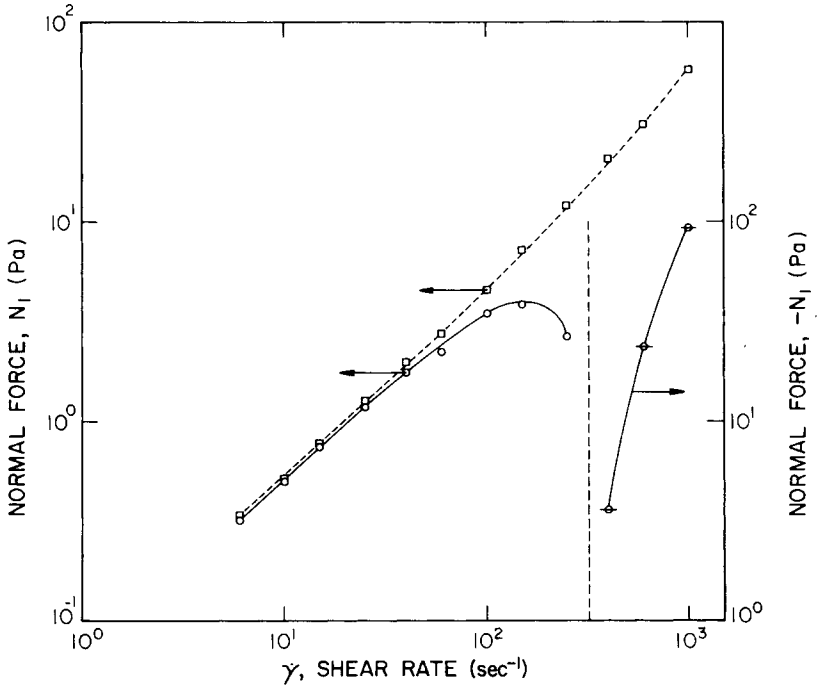


Fig. 7. Normal force correction of 2% purified guar solution: o and ⌀, uncorrected; □, corrected.

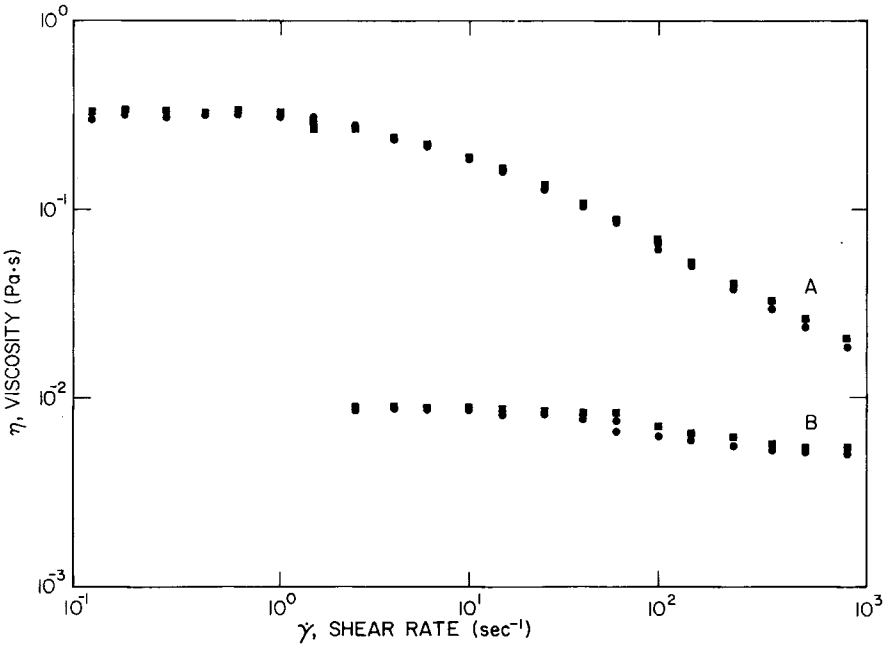


Fig. 8. Viscosity vs. shear rate: (A) 0.3% purified guar solution; (B) 0.1% purified guar solution; ●, distilled water; ■, 10% NaCl.

by Kjeldahl nitrogen) dropped 82% and the fat level (as determined by ether extractable fat) dropped 67%.

The second stage of the purification was a filtration. A water solution of the partially purified guar was made up as described in the following paragraphs. It was then filtered through an 8-$\mu$m pore diam Nucleopore membrane. This removed insoluble material, such as cellulose and other debris. The purification filtration does not shift the size distribution, but simply increases each of the peaks proportionally, due to the loss of insoluble material. Figure 4 shows a distribution plot of the hydrodynamic particle size of the purified guar in deionized and distilled water. Approximately 71% of the total sample has a hydrodynamic particle diameter between 0.2 and 0.6 $\mu$m. Material from both extremes of the unpurified guar are removed on purification, and a shift from the 0.8- through 0.6-$\mu$m to the 0.6- through 0.4-$\mu$m portion occurs. This shift in hydrodynamic particle size indicates the possibility of bundles or aggregates of guar units similar to those of cellulose or xanthan. The purified guar (as shown in Fig. 4) was used for our rheological studies.

Rheometrics torsional flow rheometer (TFR) with cone and plate fixtures was used for all our rheological measurements. The advantages of the cone and plate geometry are the following:

(1) For small cone angles, the shear stress and shear rate are nearly constant throughout the sample, and flow curves for pseudoplastic solutions can be obtained without differentiation of the data. (Our cone angles were 0.06 and 0.04 rad.)

(2) The first normal stress difference can be determined directly from the total vertical force measurement, without measuring the stress distribution in the system.

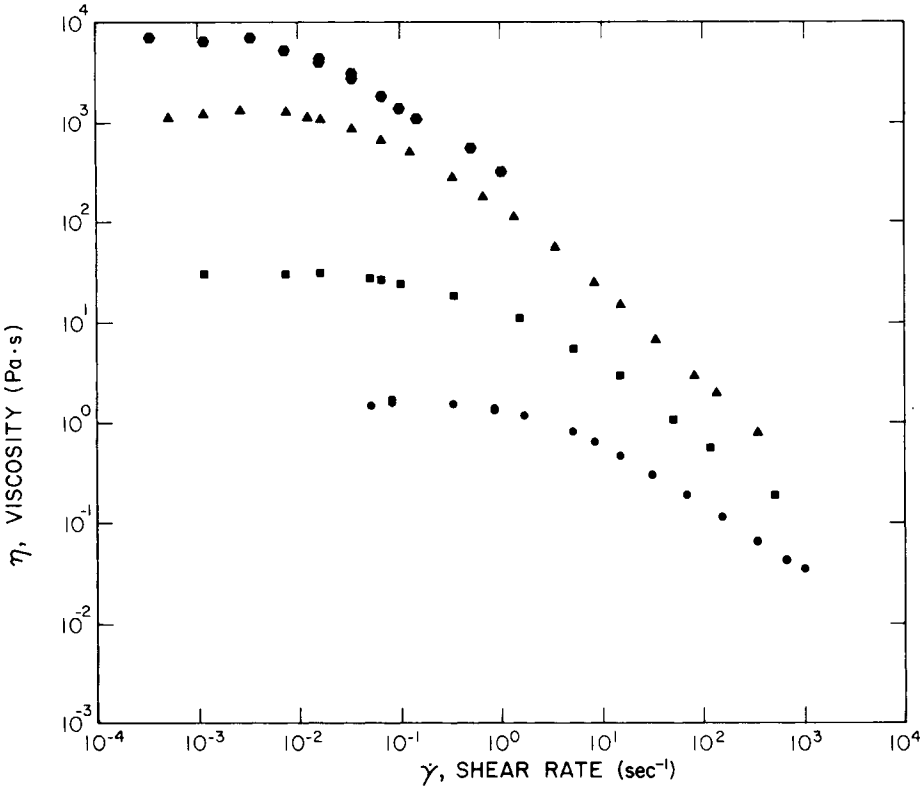


Fig. 9. Viscosity vs. shear rate, purified guar solutions: ●, 3%; ▲, 2%; ■, 1%; ●, 0.5%.

The disadvantages are as follows:

(1) Inertial forces introduce secondary flows that affect rheological measurements at high shear rates.

(2) Initially, we had problems with evaporation, i.e., surface tension. We used a cup to retain excess solution and this solved the problem.

Two transducers were used on the TFR to measure a wide range of guar concentrations. For the 0.5% and higher concentrations, we used the normal transducer with a 72-mm, 0.06-rad cone. For concentrations below 0.5%, we used Rheometric's sensitive transducer with a 50-mm, 0.04-rad cone. Figure 5, a plot of shear stress versus shear rate for a silicone oil, shows good agreement between the two transducers. Table I, which lists some physical phenomena corresponding to various shear rates, indicates the range of shear rates covered in our study.

Analysis of the cone and plate geometry is based on the assumption of a constant shear rate throughout the gap. However, Turian has shown theoretically that at high Reynold's numbers this assumption fails. Secondary flow is exhibited around the cone, adding to the measured torque. Turian's equation[3] corrects for this added torque:

$$\frac{M}{M_o} - 1 = \frac{3}{4900}\,\mathrm{Re}^2 \tag{1}$$

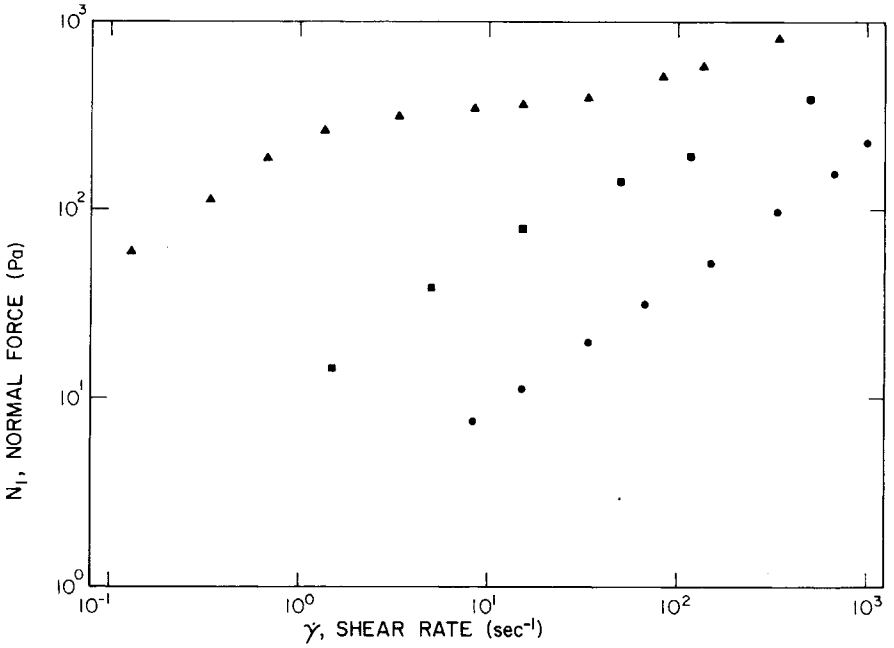


Fig. 10. Normal force vs. shear rate of purified guar solutions: ▲, 2%; ■, 1%; ●, 0.5%.

$M$ is measured torque and $M_o$ is the torque owing to primary flow. Re is the Reynold's number defined as:

$$\mathrm{Re} = \frac{\rho\omega R^2\beta^2}{\eta} \tag{2}$$

where $\rho$ is fluid density, $\omega$ is angular velocity, $R$ is the cone radius, $\beta$ is the cone angle, and $\eta$ is the viscosity.

The first normal stress difference ($N_1 = T_{11} - T_{22}$) is also affected by secondary flow, which reduces the measured normal forces. The correction for inertial effects in a Newtonian fluid[4] is:

$$(N_1)_{\text{inertia}} = -\frac{3\,\rho\omega^2\,R^2}{20} \tag{3}$$

Kulicke, Kiss, and Porter[5] have recently found this relation experimentally valid for several elastic liquids. Note that the inertial contribution is negative; hence, it must be added to the measured $N_1$:

$$N_{1_0} = N_1 + \frac{3}{20}\rho\omega^2R^2 \tag{4}$$

where $N_1$ is the measured first normal stress difference and $N_{1_0}$ is corrected for inertial effects.

Turian's torque correction is shown compared to data on water, 10-centistoke oil, and Cheng's[6] data on $n$-hexane in Figure 6. As can be seen when the measured torque is twice the primary torque, the theory overcorrects. This is not unexpected since Turian's solution is a perturbation expansion. We find that

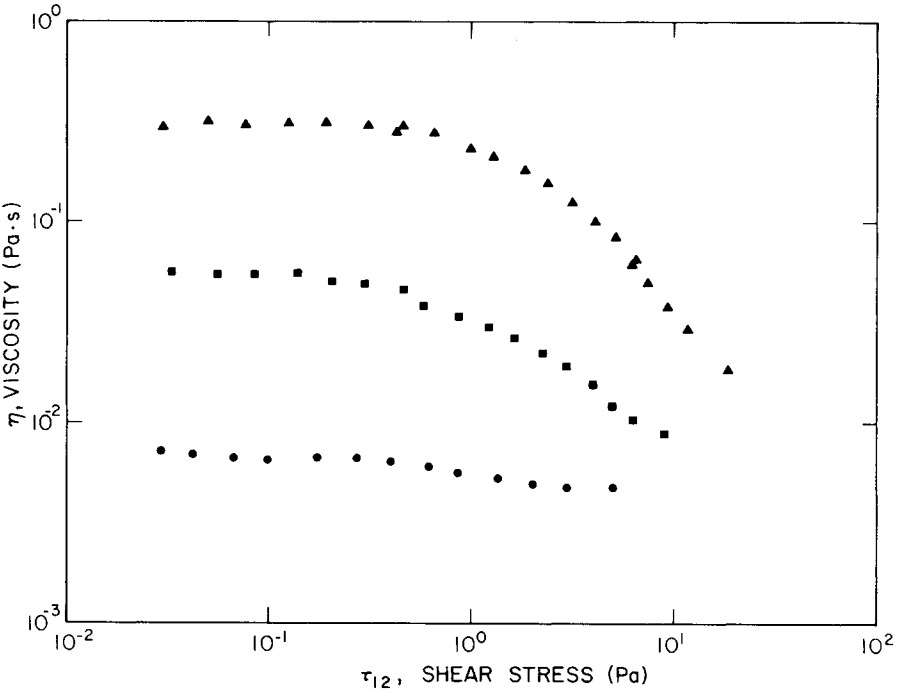


Fig. 11. Viscosity vs. shear stress of purified guar solutions: ▲, 0.3%; ■, 0.2%; ●, 0.1%.

the next term in his expansion, $-2.6 \times 10^{-4}$ Re$^4$, corrects in the wrong direction. Up to a measured value of twice the primary torque, eq. (1) was applied to our data. Although it was developed for Newtonian liquids, it appears to hold for our non-Newtonian solutions. However, we did not test this extensively.

The normal force correction is shown in Figure 7 as applied to our 0.2% guar solution. Recall that the inertial contribution to the normal force is negative and must be added to the measured normal force. (Note: The axis on the right of Fig. 7 is "negative" normal force.)

## RESULTS AND DISCUSSION

Data was taken covering broad ranges of shear rate for concentrations of 0.1–3%. Viscosity data was plotted as a function of shear rate for the higher concentrations, and as a function of shear stress for the lower concentrations. The first normal stress difference was plotted as a function of shear rate for all concentrations. On the graphs showing viscosity results the base line is the viscosity of water ($\approx$1 m Pa sec).

One feature of guar's rheology is its stability in brine solutions. Figure 8 shows a 0.1 and 0.3% solution of guar in water and 10% $NaCl_2$ solution.

Figure 9 shows flow curves (viscosity versus shear rate) for 3, 2, 1, and 0.5% solutions. Over five decades of shear rate are covered for the 1 and 2% solutions. The viscosity curve of all our solutions flattened to a constant value at low shear rates. These constant values, characterizing Newtonian regions, are known as zero shear rate viscosities, $\eta_0$. We also expect these solutions to have a Newto-

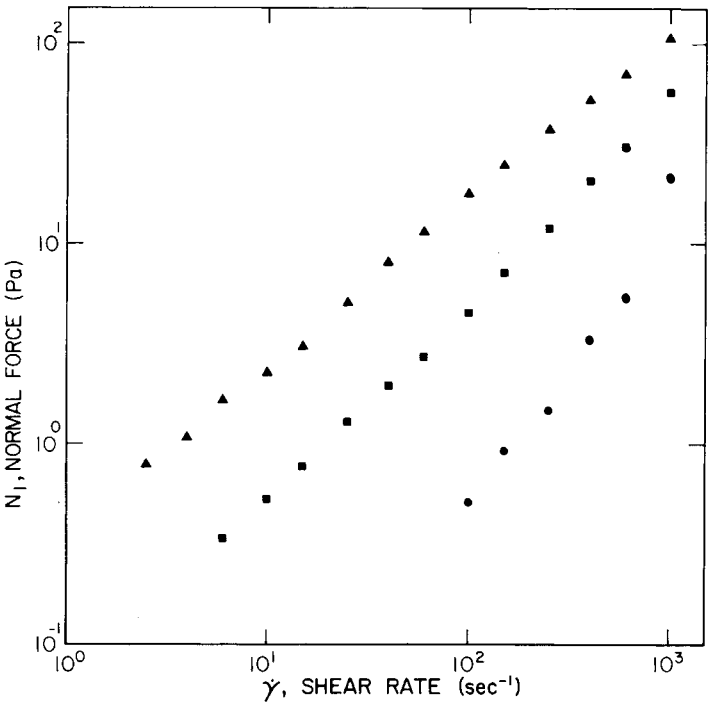


Fig. 12. Normal force vs. shear rate of purified guar solutions: ▲, 0.3%; ■, 0.2%; ●, 0.1%.

nian region at very high shear rates. This region is characterized by the infinite shear rate viscosity, $\eta_\infty$. The region between these two Newtonian plateaus is the shear thinning or pseudoplastic region. The 3% solution was very thick, and we experienced slip problems at higher shear rates; therefore, a limited shear rate range was covered. However, a Newtonian plateau at this high concentration demonstrates that guar, unlike xanthan,[7] has no true yield stress, at least up to 3% in solution. No indication of thixotropy was observed, although we did not test for it extensively.

The first normal-stress difference ($N_1 = T_{11} - T_{22}$) was measured on the 2, 1, and 0.5% solutions (Fig. 10). At the higher shear rates these were corrected for inertial effects. The presence of normal-stress differences in guar solutions imply fluid elasticity. Note that the 2% concentration appears to flatten in the middle shear rate region; this was not expected.

Viscosity is plotted as a function of shear stress for the 0.3, 0.2, and 0.1% guar solutions (Fig. 11). The plots are a function of shear stress, rather than shear rate, to show that the transition from Newtonian to pseudoplastic behavior occurs at a critical shear stress independent of concentration, at concentrations $\leq$0.3%.

The data on the 0.3% solution covers four decades of shear rate (0.1–1000 $sec^{-1}$). The viscosity of the 0.1% solution is approaching its infinite shear rate "Newtonian" plateau ($\eta_\infty$). The viscosity behavior of concentrations of guar <0.1% appears to be nearly Newtonian.

Normal-stress differences were measurable even at the 0.1% concentration of guar, Figure 12. At the lower concentrations, <0.5%, $N_1$ is directly propor-

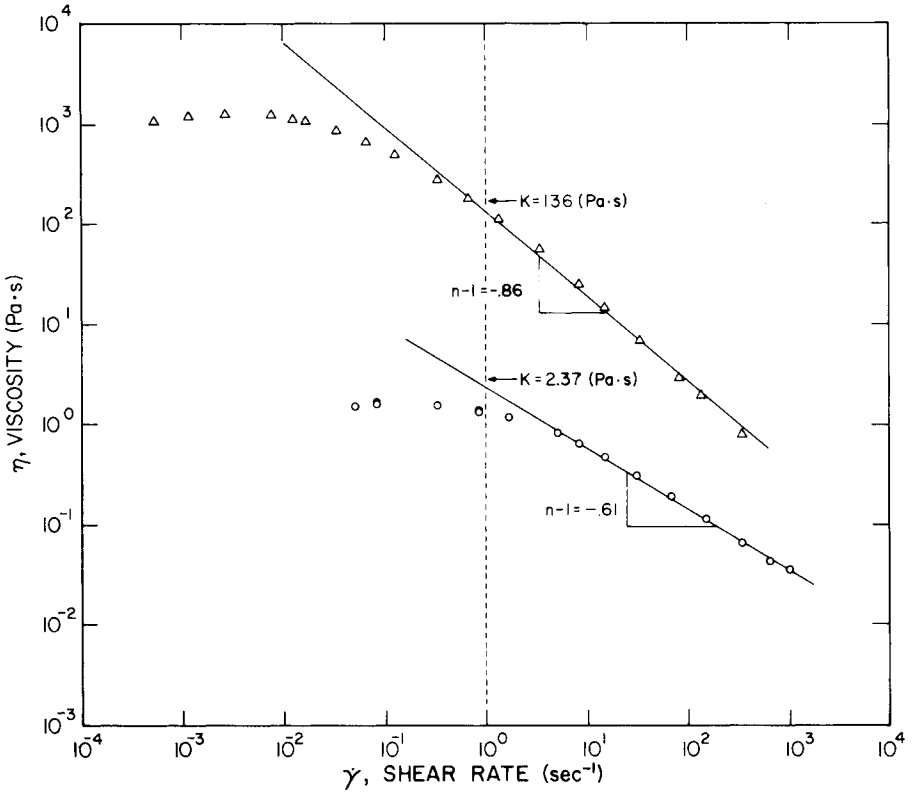


Fig. 13. Viscosity vs. shear rate of purified guar solutions showing power law fit: △, 2%; ○, 0.5%.

tional to shear rate, as opposed to the flattening observed in the 2 and 1% solutions.

Many mathematical expressions have been proposed to model the pseudoplastic behavior exhibited by guar. The most widely used is the power law of Ostwald[8]:

$$\eta_a = K\,\dot{\gamma}^{n-1}$$

The power law is appealing because of its simplicity; there are only two adjustable

TABLE II
Solution Parameters

| Concentration, % | $\eta_0$, Pa·s | $n$ | $K$, Pa·s |
|---|---|---|---|
| 3.0 | 28460 | —[a] | —[a] |
| 2.0 | 1220 | 0.14 | 136 |
| 1.0 | 31 | 0.24 | 21.5 |
| 0.5 | 1.6 | 0.39 | 2.37 |
| 0.3 | 0.31 | 0.46 | 0.733 |
| 0.2 | 0.056 | 0.60 | 0.142 |
| 0.1 | 0.007 | —[a] | —[a] |

[a] Insufficient data for meaningful estimate.

parameters, $n$ and $K$. $K$, the viscosity at 1 $sec^{-1}$, measures consistency, and $n$, the flow index, measures pseudoplasticity.

The power law fit of 2 and 0.5% guar solutions are shown in Figure 13. The model adequately represents their pseudoplastic behavior over several decades of shear rate. Note that $K$ increases with increasing concentration while $n$ decreases. Hence, the higher the concentration of guar, the more viscous the solution. However, since the higher concentration solutions are more pseudoplastic (i.e., have a lower $n$ value), the greatest difference in viscosity is at low shear rate and will decrease as shear rate increases.

The main disadvantage of the power law is its failure in the regions of very low shear rate, $\eta_0$ or $\tau_y$, and very high shear, $\eta_\infty$. More sophisticated models can account for the Newtonian plateaus in the low and high shear rate regions. For the guar concentrations we studied, the log viscosity is linear for several decades of log shear rate and is modeled well by the power law. Despite its failure in the extremes of shear rate, the power law is very useful in comparing solution properties and solving practical problems. Many empirical and analytical solutions for complex flows have been worked out using the power law; for example, laminar and turbulent pipe flow,[9] annular flow,[10] flow through porous media,[11] mixing characteristics, and heat transfer problems,[12] to cite a few. Table II gives the values for the zero shear rate viscosity ($\eta_0$) and the power law parameters ($n$ and $K$) measured at various concentrations of purified guar.

## CONCLUSIONS

From these studies the following conclusions were drawn:

(1) Guar can be purified using techniques which do not degrade its polymer portion.

(2) Guar may form bundles or aggregates in solution similar to cellulose or xanthan.

(3) Guar's viscosity is not affected by NaCl concentration.

(4) Guar solutions do not have a yield stress.

(5) Guar solutions are pseudoplastic.

(6) Guar solutions have measurable normal forces (i.e., they are not purely viscous, but exhibit elasticity).

## NOMENCLATURE

$M$ = measured torque (kg·m)
$M_o$ = torque owing to primary flow (kg·m)
Re = Reynolds number
$\rho$ = density ($kg/m^3$)
$\omega$ = rotational speed (rad/sec)
$R$ = Platten radius (mm)
$\beta$ = cone angle (rad)
$\eta$ = viscosity (Pa·sec)
$\eta_a$ = apparent viscosity (Pa·sec)
$N_1$ = first normal-stress difference (force/area)
$K$ = consistency index (units of viscosity)
$\dot{\gamma}$ = shear rate ($sec^{-1}$)
$n$ = flow index
$\tau_y$ = yield stress

$\eta_0$ = zero shear rate viscosity
$\eta_\infty$ = infinite shear rate viscosity

## References

1. R. L. Whistler and C. L. Smart, *Polysaccharide Chemistry,* Academic, New York, 1953, pp. 296–299.
2. G. Holzwarth, "Polysaccharide from Xanthomonas Campestris: Rheology, Solution Conformation, and Flow Through Small Pores" presented at the Div. of Pet. Chem. Meeting, Am. Chem. Soc., New York, April 4–9, 1976.
3. R. M. Turian, *Ind. Eng. Chem. Fund.,* **11,** 361 (1972).
4. N. Adams and A. S. Lodge, *Phil. Trans.,* **A256,** 149 (1964).
5. W. M. Kulicke, G. Kiss, and R. S. Porter, *Rheol. Acta,* to appear.
6. D. C. H. Cheng, *Chem. Eng. Sci.,* **23,** 895 (1968).
7. P. J. Whitcomb and C. W. Macosko, *J. Rheol.,* **22**(5), 493 (1978).
8. W. Ostwald, *Kolloid. Z.,* **36,** 99–117 (1925).
9. A. B. Metzner, and J. C. Reed, *AIChE J.,* **1,** 434–440 (1955).
10. P. Mishra, and I. Mishra, *AIChE J.,* **22,** 617–619 (1976).
11. R. E. Sheffield and A. B. Metzner, *AIChE J.,* **22,** 736–744 (1976).
12. W. L. Wilkinson, *Non-Newtonian Fluids,* Pergamon, New York, 1960.

Received November 1, 1979
Accepted April 25, 1980